JOURNAL OF MATERIALS SCIENCE 19 (1984) 2431–2453

Review
Adhesion and durability of metal–polymer bonds

J. D. VENABLES
Martin Marietta Laboratories, 1450 South Rolling Road, Baltimore, Maryland 21227, USA

A review is presented of those factors responsible for promoting the integrity and long-term durability of metal–polymer bonds used in the fabrication of aircraft and aerospace structures. Using a multidisciplinary approach and a variety of surface analytical techniques such as extended resolution scanning electron microscopy (XSEM), X-ray photoelectron spectroscopy (XPS), ellipsometry, and a new technique called surface behaviour diagrams (SBD), investigators at the author's laboratories have evolved several important concepts. First, it has been determined that the initial integrity of metal–polymer bonds depends critically upon the morphology of the surface oxide on the metal. For aluminium and titanium, the metals studied, it is demonstrated that certain etching or anodization pretreatment processes produce oxide films on the metal surfaces which, because of their porosity and microscopic roughness, mechanically interlock with the polymer forming much stronger bonds than if the surface were smooth. Second, the long-term durability of metal–polymer bonds is shown to depend strongly on the environmental stability (or lack of stability) of the same oxide which is responsible for good initial bond strength. For aluminium moisture intrusion at the bond line causes the oxide to convert to an hydroxide with an accompanying change in morphology and bond strength. For titanium the oxides appear to be much more stable than those on aluminium but under severe environmental conditions the oxide undergoes a polymorphic transformation which may lead to bond degradation. Third, it is observed that significant improvements in durability of adhesive bonds to aluminium can be achieved using an extremely simple treatment in which monolayer films of certain organic acids are applied to the adherend oxide to protect it against the effects of moisture.

1. Introduction

In the past, many treatments have been devised for preparing metal surfaces for adhesive bonding, painting, and the like. The general purpose of these preparation procedures is to modify the original mill surface of the metal to promote (a) development of strong bonds to polymeric materials and/or (b) better environmental stability against the effects of moisture and humidity. The degree of success in meeting these goals varies considerably, depending upon the metal involved and the process. For example, the Forest Products Laboratories (FPL) [1] process, in which aluminium is etched in an aqueous sodium dichromate–sulphuric acid solution, has been used for many years to prepare aluminium surfaces in the fabrication of adhesively bonded aircraft structures. However, more recent findings indicate that the initial integrity of aluminium–polymer bonds as well as their long-term durability can be improved considerably using the phosphoric acid anodizing treatment (PAA) [2], in which an anodizing potential is applied to the metal while it is immersed in a 10% phosphoric acid electrolyte.

0022–2461/84 $03.00 + .12

The FPL etching process, the PAA anodizing process, and, to a somewhat lesser extent, a chromic acid anodizing (CAA) process [3] have been the main pretreatment processes used for preparing the surfaces of aluminium alloys for adhesive bonding applications. The situation for titanium is somewhat different because many pretreatment processes have been developed over the years. However, until recently, none has been completely satisfactory. For example, the poor durability of adhesively bonded titanium prepared by alkaline cleaning and by the phosphate fluoride process was first pointed out by Wegman and Bondnar [4]. They subsequently developed a modified phosphate fluoride process that seemed to exhibit improved durability, but later Felsen [5] concluded that both yielded similar (marginal) results. Many other pre-treatment processes for titanium can be added to this list; some will be discussed in later sections.

The development of surface preparation methods for aluminium and titanium has in the past proceeded principally through an empirical approach in which the effectiveness of the process was tested in a more or less direct fashion by comparing mechanical properties of structures prepared using different pretreatments. Although this approach provides valuable information for ranking the pretreatment processes, it unfortunately provides little understanding of why one method is superior (or inferior) to another. More recently, however, various investigators have suggested that the microscopic roughness or morphology of the surface oxide formed in the pretreatment process is important in determining bondability. For example, Bijlmer [6], using transmission electron microscopy (TEM) to examine stripped FPL oxide films, suggested a correlation between the appearance of the oxide at high magnification and adhesive bonding behaviour. In addition, much more detailed information regarding the influence of oxide morphology on bondability was obtained by a group of investigators at the author's laboratory using the scanning transmission electron microscope (STEM) in the ultra high-resolution SEM mode [7]. The latter results have provided dramatic evidence, particularly in the form of stereo micrographs, that the morphology of the oxide plays a critical role in determining the strength of metal–polymer structures. Moreover, an extension of our initial studies has in the past several years revealed that the properties of the oxide (particularly on aluminium) play an equally critical role in determining the long-term durability of metal–polymer structures as well [8].

The comprehensive nature of and unique results obtained from our adhesive bonding investigations have suggested that it would be of interest to review our recent work and examine its broad implications in a consolidated form. This paper, in an attempt to accomplish such a goal, is therefore written along somewhat different lines than the conventional review article since the intent is to review the recent work of one group of investigators rather than to do an exhaustive review of the general literature which may be found elsewhere [9, 10]. Moreover, we further intend to introduce some previously published results which, when put in the context of examining the broad picture of adhesive bonding, will contribute significantly to the story.

Throughout the course of these investigations it was evident that the science of adhesive bonding was an area of investigation that would benefit not only from the interdisciplinary approach of physicists, chemists, materials and surface scientists, etc., but also from the proper application of sophisticated surface analytical techniques. The emphasis of this paper, therefore, is not that of a particular discipline or technique, but a synthesis of results that can be obtained when a variety of outlooks and modern equipment are used in an attempt to bring about improvements in an important technology area.

2. Role of oxide morphology

Although many factors can affect the integrity and durability of adhesively bonded metal structures, it has long been recognized that proper chemical treatment of the metal prior to adhesive bonding is essential for developing the bond strengths necessary for high-performance aircraft applications. In the past, some of these processes have been referred to as "etching" procedures with the implication that the principal function was one of cleaning the surface. Although the resulting surface is indeed cleaner than before preparation, our recent studies have shown that much more is accomplished by these pretreatment processes than is readily observed by conventional techniques. In fact, we have demonstrated that the STEM, when operated in the ultra high-resolution SEM mode (3 nm resolution compared with 10 nm resolution of a conventional SEM), is an extremely

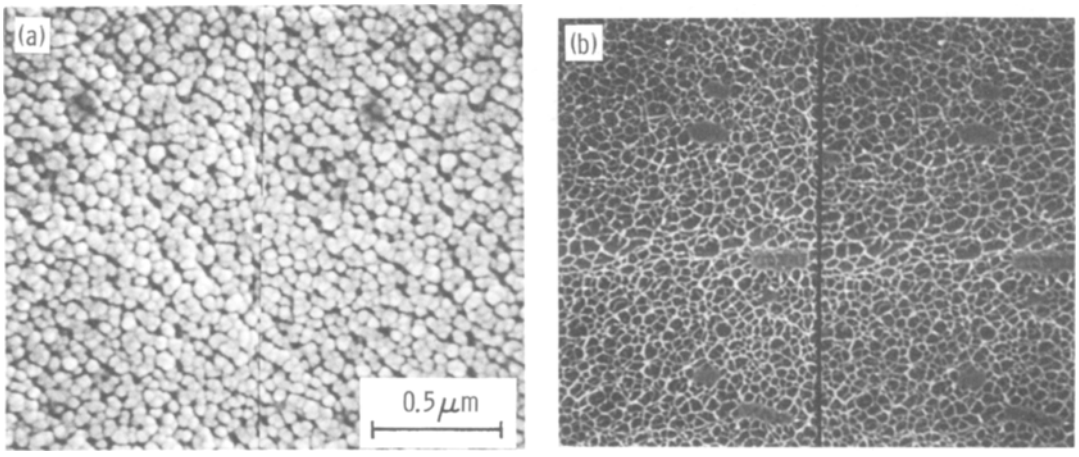

Figure 1 Stereo XSEM micrographs of an FPL-treated aluminium surface prepared (a) by gold sputtering and (b) with platinum deposited by secondary ion deposition. The spherical gold particles on the sputtered surface (a) mask the true nature of the oxide, which is revealed in (b), and in TEM micrographs, Fig. 2, taken with no coating [7].

important tool that can provide new and important information regarding the role of pretreatment processes [7]. In the following two sections, we describe observations that have been made with extended resolution SEM (XSEM) on the surfaces of aluminium and titanium prepared by various techniques.

2.1. Aluminium oxide morphology

2.1.1. Sample preparation

When we first used XSEM to investigate surfaces of aluminium prepared for adhesive bonding, we noted that sputtered gold coatings, normally used for charge bleedoff purposes on insulating materials, exhibited structures that disguised the true surface oxide morphology, Fig. 1a. Accordingly, McNamara [11] investigated the use of secondary ion deposition (SID), whereby the sample is coated with metal atoms knocked off a platinum target that is bombarded with a 5 keV argon ion beam. Platinum coatings of this type, when deposited to a thickness just adequate to bleed off charge in the microscope (~ 5 nm), introduce no significant structure up to × 200 000 magnification. In fact, the surface structure shown, Fig. 1b, is precisely that observed on stripped oxide films examined by TEM using no coating at all, Fig. 2.

We followed this procedure, using a JEOL 100Cx STEM, to perform a detailed study of the surface features resulting from preparing aluminium for adhesive bonding by the following three processes that are widely used in the aircraft and aerospace industries.

(a) *Forest Products Laboratory Process (FPL) [1]*

Following degreasing and an alkaline cleaning treatment, the panels are immersed for 15–30 min in a solution containing $Na_2Cr_2O_7 \cdot 2H_2O$, H_2SO_4 and H_2O in a 1:10:30 ratio by weight. The bath temperature is maintained at 68° C.

(b) *Boeing phosphoric acid anodize process (PAA)[2]*

The panels are treated first by the FPL process and then anodized at 10 V for 25 min in an aqueous solution containing 10% by weight of H_3PO_4. The bath temperature is maintained at 24° C.

(c) *Chromic acid anodize process (CAA)[3]*

The panels are treated first by the FPL process and then anodized with step-wise voltage application

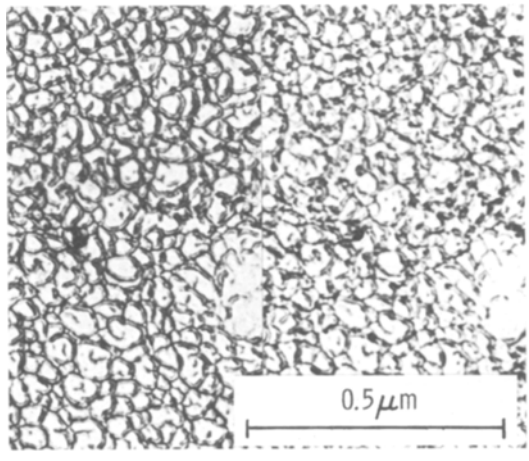

Figure 2 Oxide morphology of FPL-treated aluminium observed in stereo by TEM on stripped oxide films [7].

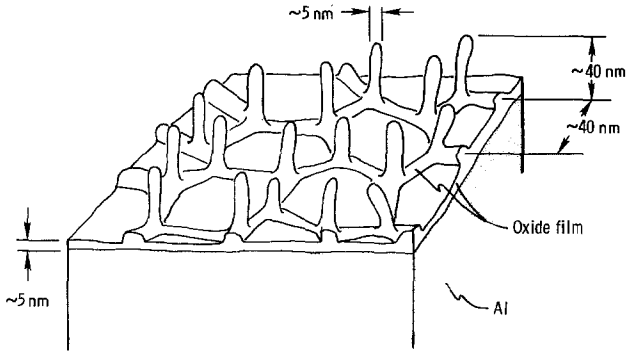

Figure 3 Perspective of the oxide morphology produced on aluminium by the FPL process [7].

in an aqueous solution containing 5% by weight of CrO_3. The bath temperature is maintained at 40° C. Eight 5 V steps are applied within 10 min, the panels are held at 40 V for 20 min, and then the voltage is increased to 50 V within 5 min and held for an additional 5 min.

2.1.2. FPL process

Stereo pairs of the three-dimensional oxide morphology formed by the FPL process on 2024-T3 aluminium are shown in Fig. 1b which was taken with XSEM at x 50 000 direct magnification using a platinum charge bleed-off coating. To emphasize the high resolving power of the technique, we can compare the stereo-XSEM micrograph with that in Fig. 2 which was taken with a conventional TEM using no charge bleed-off coating. In the latter, the oxide was stripped from the aluminium by dissolving the substrate in an aqueous solution containing 10% $HgCl_2$. It is evident that the high-resolution XSEM technique provides images of important fine details which are similar in quality to those obtained with a TEM. Because the XSEM technique requires very little sample preparation and can be used to examine the structure of thick oxides, it is a powerful tool for this application.

Our interpretation of the FPL oxide morphology is shown in Fig. 3. In the drawing, the FPL oxide is characterized by a cell structure and a high concentration ($\sim 10^{10}$ cm^{-2}) of 5 nm thick, 400 nm high oxide whiskers that protrude from the surface. The microscopic interlocking roughness exhibited by the structure is apparently a crucial factor determining adhesion at the epoxy–oxide interface in bonded aircraft structures. To demonstrate this, we intentionally added 500 ppm fluorine to the etch bath. We observed that the surface oxide morphology was drastically modified, becoming much less interlocking in nature, Fig. 4. This surface exhibits undulations, but does not interlock with polymeric coatings. It may readily be separated from an overlying adhesive or primer coating to allow examination of the polymer side of the interface. When this is done, the polymer

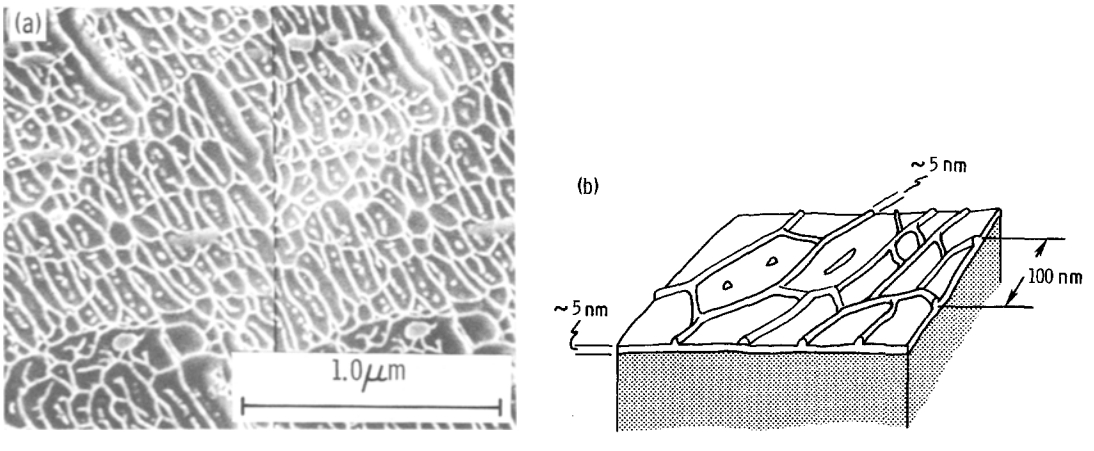

Figure 4 (a) Stereo pair and (b) perspective drawing of oxide morphology of aluminium surface prepared with an FPL solution contaminated with 500 ppm F. The oxide surface is considerably less interlocking than that of the normal FPL oxide shown in Figs. 2 and 3.

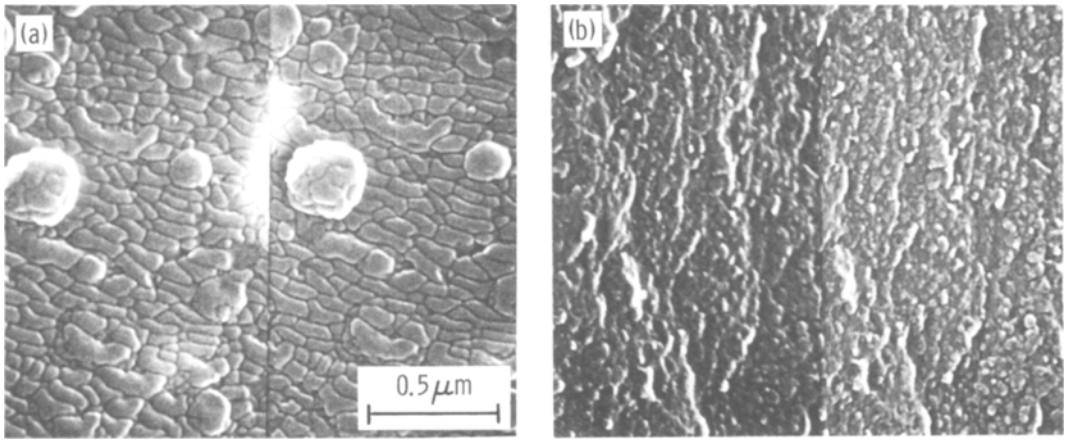

Figure 5 Stereo XSEM micrographs of an epoxy adhesive separated from (a) an oxide prepared in an FPL solution contaminated with 500 ppm F and (b) a normally prepared FPL oxide.

retains a perfect replicate of the original oxide features, Fig. 5a. This situation contrasts in two respects with the behaviour exhibited when attempts are made to separate a normally-prepared FPL surface from an overlying adhesive. First, separation at the oxide–polymer interface is much less easy to achieve if the metal is properly prepared (but can be done if the aluminium is first bent very sharply). Second, the separation of good bonds, when forced to occur at the oxide–polymer interface, is accompanied by an extreme amount of deformation of the polymer which is generally badly torn and ripped, Fig. 5b. One consequence of this different mode of separation is that the bond strength, as measured by a climbing drum peel (CDP) test [12], for example, may be as much as a factor of three different, with the interlocking surface yielding the highest strength levels. Another consequence of not having an interlocking morphology is that the peel strength can be lowered further simply by placing a drop of water in the crack developed during the test. We interpret this to mean that in the absence of mechanical interlocking, when the bond strength is determined principally by chemical forces across the interface (e.g. Van der Waals or dispersion forces), the presence of water can disrupt these bonds readily, thereby reducing the interfacial strength. A similar effect is observed for mica, which is bonded across the layer planes by Van der Waals forces. When cleaved in a wet environment the fracture energy of mica is two to four times lower than when done in a dry environment [13]. For adhesive bonds, however, water has no significant short-term effect when interlocking is present. (The long-term effect of moisture on properly prepared bonds will be discussed in Section 3).

Although fluorine picked up from the contaminated bath and deposited on the oxide surface might be responsible for the observed degradation in bond strength, examination by Auger/ESCA of surfaces prepared in fluorine-contaminated baths indicated that the surface concentration of fluorine was very low (less than 3% surface coverage). Prior work [14], in which fluorine was added to rinse water (in which case, much higher concentrations of fluorine can be adsorbed on the surface), has demonstrated that such low concentrations of fluorine, *per se*, do not significantly degrade bond strength so long as the oxide morphology is not altered.

The roles of mechanical interlocking and chemical bond formation in adhesive bonding have been a subject of much discussion [15–19]. In the present case of FPL-etched aluminium surfaces bonded to epoxy adhesives, the role of mechanical interlocking appears to be particularly important. Moreover, it should be emphasized that the effect is not due solely to an increased surface area. Although the existence of protrusions does increase the interfacial area available for chemical bonding, we can estimate, from their dimensions and density, that the protrusions on an FPL-treated surface increase the interfacial area by only 10% whereas they can increase the CDP strength three-fold. The interlocking nature of the rough oxide apparently is responsible for achieving good bondability.

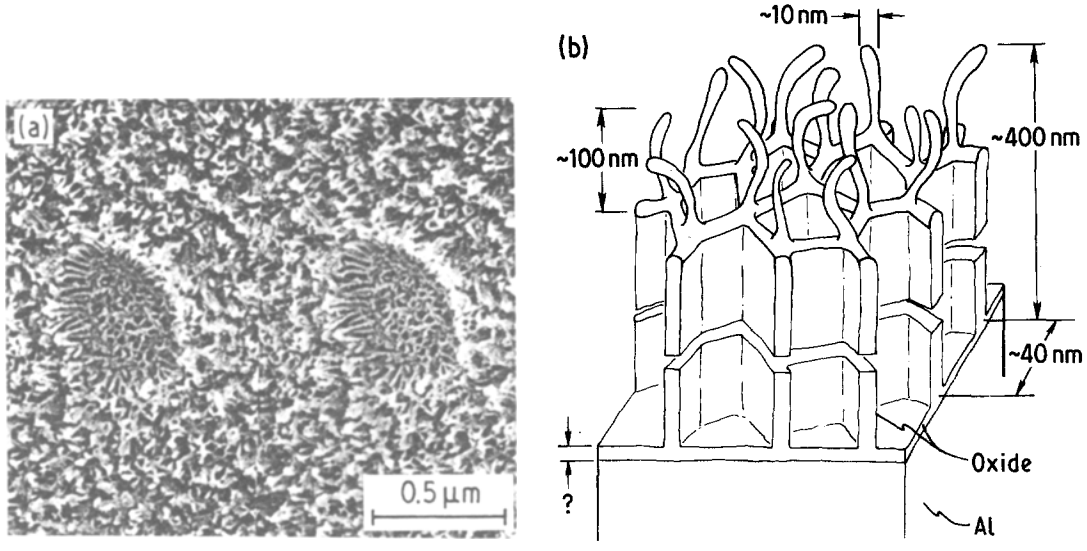

Figure 6 (a) Stereo XSEM micrograph and (b) isometric drawing of the oxide morphology on a PAA-treated aluminium surface. The origin of the depressed region in the oxide seen in (a) is unknown, but may have been due to a gas bubble or inclusion that inhibited oxide growth [7].

2.1.3. PAA process

The PAA process for preparing aluminium adherends for bonding produces an oxide morphology, shown in Fig. 6, that is different in a number of respects from that associated with the FPL process. Specifically, (a) the oxide produced by anodization is considerably thicker; (b) the hollow hexagonal cell structure, which exhibits a low profile in the FPL oxide, is much better developed in the PAA films; and (c) the whisker-like protrusions are considerably longer on the PAA-treated surface.

The morphology shown in Fig. 6 also differs in a significant manner from that of earlier models. Although the existence of hollow hexagonal cells on anodized aluminium surfaces is well established [20], to our knowledge the existence of protrusions above the hexagonal structure has not been appreciated prior to our reporting it [7]. In the present work, therefore, we introduce the concept of a "fibre-reinforced interface" that may be very important in determining bondability.

Because of its more fully developed structure, the PAA surface might be expected to provide better mechanical interlocking to a polymer and therefore exhibit a stronger bond than the FPL surface. This is consistent with test data comparing PAA and FPL surfaces, as reported by Kabayashi and Donnelly [2]. It is also consistent with observations McNamara [21] has made concerning the depth to which epoxy primers and adhesives penetrate into the PAA oxide. In his work, 6061 aluminium panels were prepared using the standard PAA process and then coated with an adhesive-based primer (BR-127 American Cyanamid) that was applied according to specifications. The aluminium was then bent sharply until the primer cracked, thus allowing a cross section of the oxide–primer interface to be observed with XSEM as shown in Fig. 7. The micrograph reveals that the primer has penetrated completely into the porous oxide leaving absolutely no voids or empty regions even at the bottom of the pores. We suspect that the high degree of penetration is caused by strong capillary forces and that the wettability between the polymer material and the oxide plays an important role in achieving penetration. This assigns a somewhat more indirect role to the wettability factor than it ordinarily receives. Conventionally, good wettability is assumed necessary to achieve good bond strength because it implies a good chemical bond across the interface. This is undoubtedly a critical factor in the case when bonds are made to smooth surfaces. However, for porous surfaces the effect may be one of promoting penetration of the polymer to maximize the degree of interlocking and thereby achieve a stronger bond.

Since the porous nature of the PAA oxide appears responsible for the success of this pretreatment process for promoting strong adhesive bonds to aluminium, Ahearn *et al.* [22] have

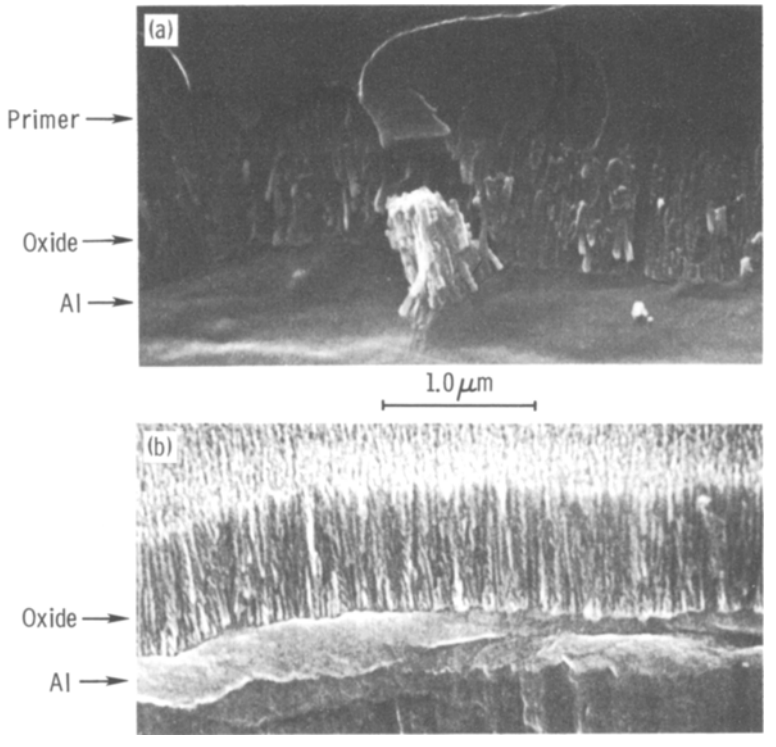

Figure 7 Cross-sectional views of PAA-prepared aluminium surface (a) with and (b) without overlaying primer. Penetration of the primer into the pores of the PAA oxide is so complete (a) that the oxide is difficult to see.

investigated the kinetics of oxide growth and development of the whisker-like oxide morphology. Their intent was two-fold: (a) to learn how processing parameters affect the oxide morphology, and (b) to satisfy a basic curiosity regarding the formation mechanism. The results of their study demonstrate that the development of the porous oxide structure is characterized by a two-stage process (Fig. 8) involving a fast, linear growth stage during which the pore cell structure forms, followed by a slower stage during which fine "whiskers" are formed on top of the cells. Pore development appears to be accomplished by field-assisted dissolution across a barrier layer at the root of the pores in a manner consistent with the theory of Hoar and Mott [20]. The evidence we have obtained to support this field-assisted dissolution hypothesis may be summarized as follows: When a film is first anodized to a potential of say, 8 V, and then the potential suddenly is reduced to 4 V, the current drops drastically and remains at a low value for about three minutes after which it increases to reach an equilibrium value characteristic of the newly applied potential. During this incubation time a new (thinner) equilibrium barrier oxide thickness is established by dissolution of the oxide. The rate at which the barrier film was reduced in thickness with voltage applied was compared with the situation with no power on by first anodizing to 8 V as above, turning the power off, soaking the sample in the electrolyte for 5 min, and then applying the 4 V potential. Even though the unpowered soak time was greater than the original power-on incubation time, we nonetheless observed that the 4 V potential had to be applied for an additional 2.5 min before the current rose to its equilibrium value.

This result and others discussed by Ahearn *et al.* [22] substantiate the prevailing theory of pore growth, which emphasizes field-assisted dissolution as a key mechanism [20]. According to this theory, once the porous structure initiates, each pore grows by preferential oxidation and dissolution at the bottom of the pore where the field strength is greatest. Pore initiation always occurs after the anodization current density drops to a value close to the steady state current density or, correspondingly, after the barrier grows to a nearly steady-state thickness. The process is then limited by the oxide dissolution rate, which remains constant as long as the field across the barrier and the active ions in the pore (e.g. OH^-, Al^+) remain unchanged. This is probably the situation during the first stage of the two-stage process for PAA depicted in Fig. 8.

Dissolution of the oxide in a field-free region

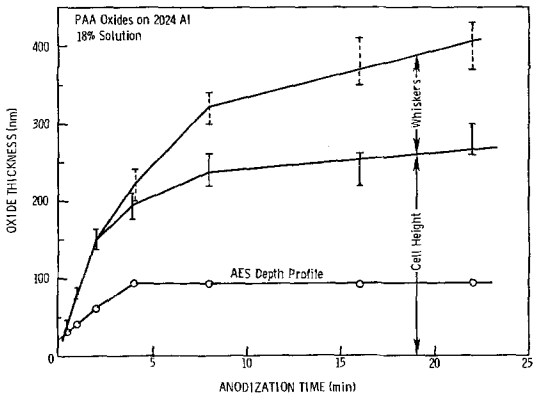

Figure 8 PAA oxide thickness as a function of anodization time determined by STEM (vertical bars) and AES depth profile (circles).

depends strongly on the concentration of the active ions. A noticeably high H^+ concentration enhances dissolution, whereas a higher Al^{3+} concentration tends to reverse the reaction. The effect of PO_4^{3-} is not well understood, but is believed to retard aluminium dissolution [23]. When a field is applied, the high dissolution at the pore bottom provides a constant supply of Al^{3+} inside the pore, while also driving PO_4^{3-} ions into the oxide pore and H^+ ions away from the oxide. As a result, the dissolution of the oxide throughout most of the porous layer is small. Alternatively it is expected that the outer extremities of a thick oxide will dissolve at a higher rate than the mean because of the general availability of H^+ ions and a reduced concentration of Al^{3+} ions.

The above dissolution characteristics may be used, at least tentatively, to describe the mechanisms of the transition from the first stage to the second stage. When the pore develops to a certain critical depth (depending on solution concentration and applied field), the ridge of the cell wall that is located away from the source of the Al^{3+} ions, and, therefore, faces the electrolyte, will begin to dissolve at a relatively fast pace. The wall between two adjacent cells is thinner than the intersection of three walls so that as the dissolution proceeds, the walls are consumed first, leaving behind the skeleton of the intersection, which is then seen as whiskers in the second stage of oxide film growth. It is important to point out that although the second stage of oxide growth appears to proceed at a lower rate than the first stage, the anodization and dissolution processes at the barrier region must proceed at nearly a constant rate in both stages because of no observable change in the anodization current density. The apparent slow-down in the oxide growth is due to the fact that dissolution of the outer porous layer more effectively balances the growth of the oxide at the barrier layer as anodization proceeds.

Although the mechanism by which the pores initiate is a very important but unknown factor in anodization, we have not addressed this issue in our work. Clearly, further studies to clarify the nucleation mechanism are needed.

2.1.4. CAA process

The oxide produced by the CAA process differs in several significant ways from those formed by the FPL or PAA processes. First, the CAA oxide is considerably thicker (~ 1000 nm) than either the FPL (~ 40 nm) or PAA (~ 400 nm). This difference is undoubtedly related to the high voltage and long anodization times used in the CAA process. Second, although the CAA oxide does exhibit some bulk porosity, the wall thickness is greater, and the pore size smaller than for PAA films. Third, the surface morphology of CAA oxides varies depending upon the prior history of the aluminium being anodized. For example, if the aluminium is first treated by the FPL or PAA process, then the morphology characteristic of these pretreatment processes is retained at the top surface of the CAA oxide (Figs. 9a and b). Moreover, if the initial oxide is smooth like a thermal oxide, then the surface of the anodic oxide is also smooth (Fig. 9c). Evidently, the new oxide grows underneath the old, pushing the old one up as the new one grows in height.

The observation that the outer surface morphology of the CAA oxide depends on the initial condition of the surface oxide suggests that the bondability to CAA-treated aluminium likewise would depend on the type of oxide present before anodization. For example, bondability would be expected to improve significantly if the surface were first treated by the PAA process rather than by the FPL process currently used. This situation contrasts markedly with our observations regarding the FPL and PAA processes, which indicate that the oxide morphology developed is quite independent of prior surface preparation since the original oxide is dissolved away during the initial stages of the respective treatments. (An FPL oxide dissolves completely within 30 sec after immersion in the PAA electrolyte.) Clearly, these consider-

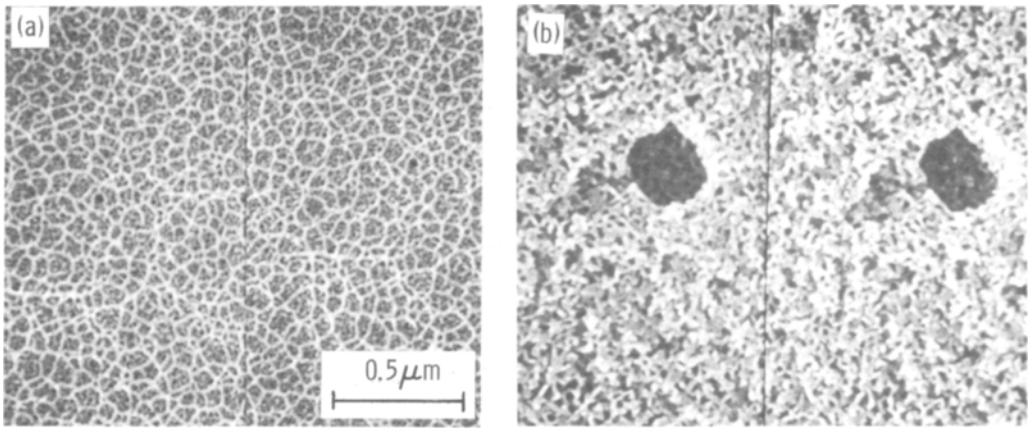

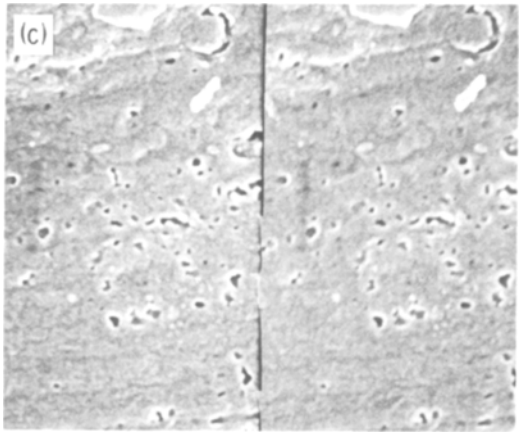

Figure 9 Stereo XSEM micrographs of oxide morphology on CAA-treated aluminium samples which have been pretreated by the (a) FPL process, (b) PAA process, and (c) tartaric acid anodization. The success of the CAA process for adhesive bonding is expected to depend strongly on the pretreatment process.

ations must be taken into account if acceptable and reproducible results are to be obtained from the CAA process.

2.2. Titanium oxide morphology

Although considerable success can be achieved in bonding polymers to aluminium using either the PAA or FPL pretreatment process, the situation is not as straightforward for titanium. Prior attempts to develop as successful a pretreatment for titanium have yielded many processes, but not until recently have any shown promise. Because of the increasing interest in using titanium for advanced aircraft structures we believed it was important to know more about the types of surfaces generated by these processes with the hope that this information would provide guidelines for future improvements. Accordingly, using the techniques we employed for studying aluminium adherends, Ditchek *et al.* [24] characterized titanium surfaces prepared by various pretreatment processes. The results were then compared with measurements of mechanical properties performed by other investigators [25] in a coordinated US Navy (NAVAIR) program as discussed in the next sections.

2.2.1. Characterization of titanium adherends

The various surface pretreatments and the types of surfaces generated on Ti–6Al–4V alloys are shown in Table I. The references provide details of the preparation procedures. Although the surfaces varied considerably, they could be classified into three groups according to morphology. Group I surfaces, which include those resulting from the PF and MPF treatments (notation defined in Table I), display little macro- or microroughness.* Group II surfaces, which derive from the DA, LP, TU and DP treatments, all exhibit a large degree of macroroughness; the LP and TU surfaces also exhibit a small degree of microroughness. Group III surfaces, which include those generated by chromic acid anodization at 5 or 10 V, are characterized by having no macroroughness, but a high degree of microroughness associated with a porous oxide.

The Group III surface morphologies are of particular interest because of their marked resemblance

*A macrorough surface is defined as an uneven surface with characteristic bumps or jagged features about 1.0 μm or greater. Microrough surfaces have fine structure with dimensions 0.1 μm or less.

TABLE I Morphological characteristics and chemical contaminants associated with various titanium pretreatment processes

Process	Process code	Reference	Oxide thickness (nm)	Group number*	Comments
1. Phosphate fluoride	PF	[4]	20	I	F contamination
2. Modified phosphate	MPF	[4]	8	I	F contamination
3. Dapcotreat	DA	[26]	6	II	No apparent fine structure, Cr on surface
4. Dry hone PASA JELL 107	DP	[27]	10 to 20	II	Deformed surface with embedded Al_2O_3, fluorine contamination
5. Liquid hone PASA JELL 107	LP	[27]	20	II	Embedded alumina, fluorine contaminant, Cr on surface
6. Turco 5578	TU	[27]	17.5	II	Fe-containing particles on surface
7. Chromic acid anodize	CAA	[28]	5 V:40 10 V: 80	III III	Porous oxide with protruding whiskers, fluorine contamination

*For a definition of group numbers, see text.

to those produced on aluminium by the PAA or FPL process. For example, the CAA surface on titanium exhibits a porous oxide with protruding whiskers similar to the FPL structure and is approximately the same thickness if the anodizing potential is 5 V and the anodization time is 20 min. When the anodizing potential is raised to 10 V (and the time remains the same), the surface morphology becomes somewhat intermediate between that of FPL and PAA oxides in both appearance and thickness (Fig. 10). Because of these similarities, it would therefore be expected that the CAA oxides would interlock with polymer coatings, providing interfacial bond strengths comparable to those associated with aluminium prepared by the FPL and PAA processes.

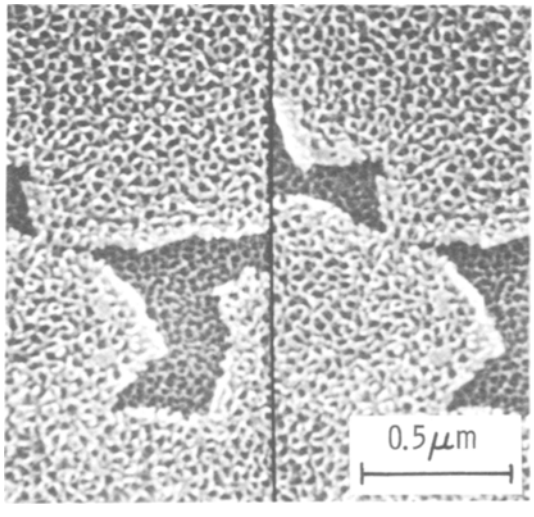

Figure 10 Stereo XSEM micrograph of the oxide on titanium produced by the CAA process [24].

Evidence that this is the case is provided by wedge tests performed by Brown [26], who prepared titanium surfaces the same way as for XSEM examination. A standard wedge test configuration [29] was employed using the BR127/FM300 primer/adhesive system to bond the titanium test strips together. In this test, two thick adherends given identical surface preparation are primed (if desired) and then bonded together. Stress is applied to the bondline by driving a wedge between the adherends, and the growth of the crack induced in the bondline is visually monitored along the bondline as a function of exposure time in elevated temperature and humidity conditions. Correlations between rapid crack growth and poor in-service performance observed in aircraft components have been established [30]. The predictive value of this simple test has been widely accepted by the aerospace industry [31]. The test conditions and results are indicated in Fig. 11.

This work clearly demonstrates a correlation between surface roughness and bond strength. Thus, the Group I surfaces, having no macro- or microroughness, exhibit very poor behaviour in the wedge test with all of them failing adhesively at the primer–metal oxide interface. On the other hand, the Group III surfaces, having no macroroughness but a high degree of microroughness in the form of porous oxides, exhibited almost no crack growth except for a small amount of cohesive failure in the adhesive during early stages of the test. The wedge test values corresponding to the Group II category are intermediate between the two other Groups which is consistent with the

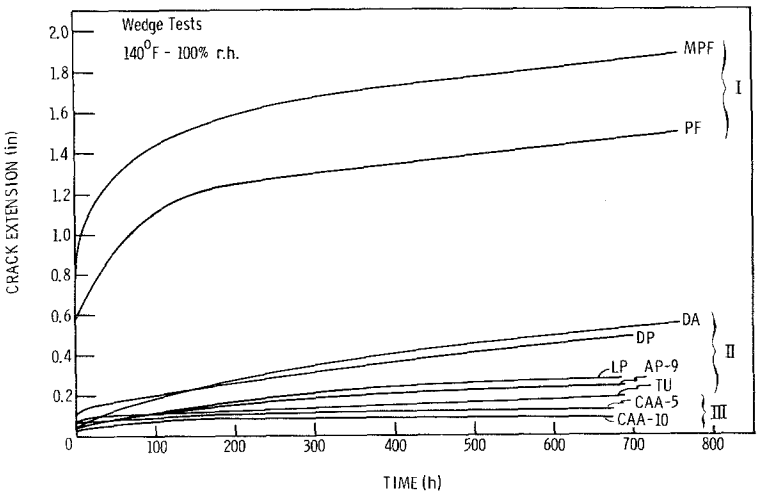

Figure 11 Results of wedge tests on titanium suggesting that adherends with high surface roughness and the ability to mechanically interlock with the adhesive provide the most durable bonds. Definitions of Groups I, II and III can be found in the text [26].

fact that Group II oxides exhibit more macroroughness than Group I but less microroughness than Group III. Evidently, the presence of a porous oxide that can interlock with the polymer is just as important a factor determining the strength of polymer bonds to titanium as is the case for aluminium.

Finally, we note that the alkaline peroxide (AP) process [32] also shows considerable promise, but we will defer further discussion since our work on it is incomplete.

3. Environmental stability of oxide surfaces

In the previous section we discussed the important role that oxide morphology plays in determining the bond strength of adhesively bonded aluminium and titanium structures. In this section we discuss the role that the stability of the oxide in moist or wet environments plays in determining the long-term durability of metal–polymer bonds.

3.1. Stability of oxides on aluminium

Our interest in the stability of those oxides that are responsible for promoting strong metal–polymer bonds arose when we first investigated failed surfaces of aluminium wedge test samples with XSEM. The samples used for the wedge tests usually were 2024-T3 aluminium prepared by the FPL process initially, and in later experiments by PAA anodization. The bond was made with the adhesive (FM123-2) contacting the adherends directly, i.e. no primers were used in the experiments.

Under these accelerated test conditions, and with the humidity chamber at 65° C and 100% r.h., the crack immediately travelled along the adhesive–oxide interface; it had initially propagated through the middle of the adhesive. Examination of the crack interface with XSEM surprisingly revealed no remnants of the original oxide morphology on the adherends. In fact, we observed that the surface morphology had been converted from that shown in either Fig. 3 (FPL) or Fig. 6 (PAA) to a new morphology of the type shown in Fig. 12. In addition, we observed that the adhesive side of the interface exhibited the same morphology and presumably was also covered with the same material.

A detailed analysis of the material shown in Fig. 12, using high-resolution X-ray photoelectron spectroscopy (XPS) (also known as electron spectroscopy for chemical analysis (ESCA)) to monitor chemical shifts, indicated that the substance on both sides of the crack interface was aluminium hydroxide with a chemical composition (determined by measuring the Al/O ratio) between that of boehmite ($Al_2O_3 \cdot H_2O$) and pseudo–boehmite ($Al_2O_3 \cdot 2H_2O$). This identification was later confirmed using electron diffraction, which gave a crystalline ring pattern consistent with that of boehmite. By way of comparison, it should be noted that electron diffraction patterns obtained from stripped FPL or PAA oxide films exhibit only two extremely diffuse rings, indicating that the original oxides are quite amorphous.

Evidence that the failure of the bond was caused directly by the conversion of oxide to hydroxide was obtained by measuring the hydroxide layer attached to the adhesive side. It was 60 nm thick whereas the effective thickness of the original FPL oxide was ~ 20 nm. (The effective thickness measured by Auger depth profiling is somewhat less than the overall thickness shown

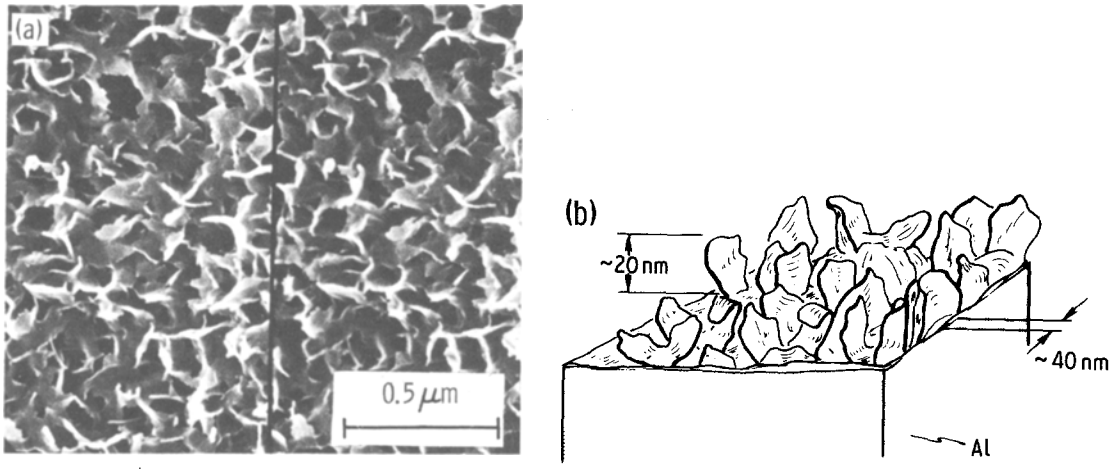

Figure 12 (a) Stereo XSEM micrograph and (b) isometric drawing of aluminium hydroxide (pseudo-boehmite) produced on aluminium surface during wedge test or exposure to moisture [8].

in Fig. 3.) According to Veddar and Vermilyea [33], the conversion of aluminium oxide to hydroxide is accompanied by a threefold increase in thickness. Thus, there is a strong suggestion that the hydroxide sticking to the adhesive was formed directly from the original FPL oxide on the aluminium. Evidently, the adhesion of the hydroxide to aluminium is sufficiently weak that once the hydroxide forms, it separates from the adherend giving rise to bond failure. The newly exposed aluminium surface then hydrates further as the crack opens up. This proposed failure model is shown schematically in Fig. 13.

3.1.1. Hydration studies

If the proposed failure mechanism for adhesive bonds in a humid environment is correct, we would expect a correlation between hydration rates of the oxide surfaces and wedge test results. In this section we describe results of hydration studies using ellipsometry and XSEM and compare them with wedge test performance.

Although XSEM is a powerful tool for observing changes in the oxide when it hydrates, it is not amenable to making real-time measurements of hydration rates. For this purpose we chose to use ellipsometry, a technique that is very sensitive to surface changes such as those that are associated with the oxide-to-hydroxide conversion. The ellipsometer, shown schematically in Fig. 14, has three major optical components: the polarizer, the compensator, and the analyser. The compensator converts the incoming plane-polarized light into elliptically polarized light characterized by two perpendicular energy vectors that differ in phase. The polarizer can adjust this phase difference so that it exactly compensates for the phase shift that occurs upon reflection from the sample. The analyser then extinguishes the now plane-polarized beam reflected from the sample surface. In practice, the compensator is fixed at 45°, and the polarizer and analyser are rotated to accomplish extinction. The point of extinction represents a null point in light intensity that is specific for the thickness and optical constants of the oxide film on the sample surface.

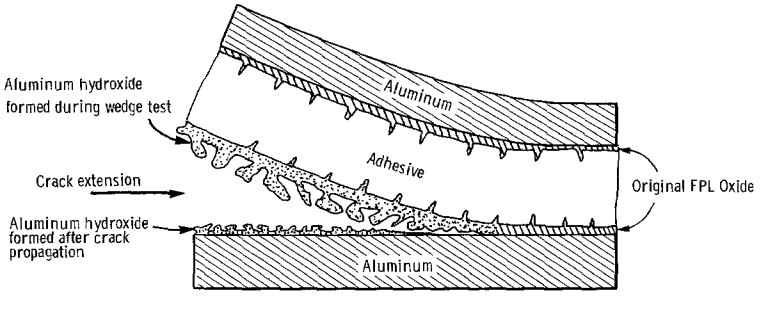

Figure 13 Schematic drawing of the mechanism deduced from crack propagation during wedge testing. In the humid environment, the original oxide is converted to a hydroxide which adheres poorly to the aluminium substrate. The crack propagation rate is faster here than in a dry atmosphere, where the crack propagates directly through the adhesive [8].

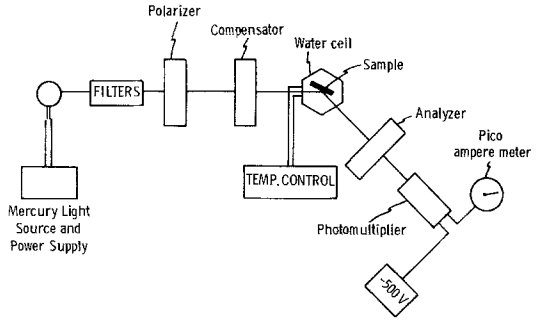

Figure 14 Schematic diagram of an ellipsometer. Monochromatic, elliptically polarized light reflects from the sample in the temperature-controlled cell during hydration. The analyser is adjusted initially for minimum light intensity and any change in the surface, e.g. hydration, causes an increase in intensity.

For our experiments we immersed the specimens in a temperature-controlled water cell having optical windows and set the null point for the unhydrated surface. Thus, any subsequent change in the surface film due to hydration activity causes an increase in the detected light intensity. Monitoring the photomultiplier output during water immersion allowed us to determine the time interval before the specimen began to hydrate.

A typical measurement made on FPL-treated 2024-T3 aluminium exposed to 80° C deionized water is shown in Fig. 15, along with XSEM stereo micrographs that depict the evolution of morphological changes as a function of exposure time. The data and micrographs indicate that there is an incubation time of approximately two minutes during which the optical properties and appearance of the oxide change very little. Beyond this time, the oxide surface begins to hydrate: First, the oxide porosity begins to fill in, Fig. 15b, and the surface begins to roughen considerably (Fig. 15c); and then the characteristic "cornflake" structure of the pseudo-boehmite develops, (Fig. 15d) by the reaction:

$$Al_2O_3 + H_2O \rightarrow 2AlOOH \qquad (1)$$

After this point, we begin to see gas evolution, suggesting that the aluminium metal has come into contact with the water and is corroding by the reaction:

$$2Al + 4H_2O \rightarrow 2AlOOH + 3H_2\uparrow \qquad (2)$$

Evidently, the conversion of the original oxide to a hydroxide may lead not only to the degradation of adhesive bonds but also to the general corrosion of aluminium. Thus, if the first step, oxide-to-hydroxide conversion, were inhibited, then the subsequent step, corrosion, would likewise be inhibited. We will return to this important point in later sections.

Using the incubation time associated with the hydration process as a criterion for evaluating the stability of oxide surfaces, we have measured this value for various types of surfaces and compared the results with wedge test data to determine whether there is a correlation [34]. In measuring the incubation time for PAA surfaces, we found it was considerably greater than the two-minute incubation time for FPL surfaces. Much scatter was observed in the data, with values ranging from 15 min to 16 h; the most frequently observed times were between 3 to 5 h. This difference in incubation times for FPL and PAA is consistent with wedge test results of Kabayashi and Donnelly [2] who reported that the wedge test performance on PAA-treated adherends was far superior to that for FPL. Therefore, a qualitative correlation between the stability of surface oxides on aluminium and wedge test performance is suggested.

A more quantitative correlation was obtained in studies which were originally intended to test the effect on wedge tests of exposing aluminium adherends to conditions used for curing high-temperature adhesives. In this work, we noted that wedge test results for an adherend made from a magnesium-containing alloy, such as 7075, improved as the high-temperature soak time increased. Thus, for the present work, 7075-T6 adherends were given an FPL treatment and then heated in air at 180° C for up to 5 h. Although XSEM examination of the treated surfaces indicated no detectable physicla change, Auger analysis indicated a significant increase in the magnesium content of the FPL oxide as the heat treatment time increased.

Wedge test performance of adherends prepared in this manner generally improved with increasing heat time, as shown in Fig. 16, which we tentatively attribute to the increased magnesium content of the oxide. However, we cannot discount the possibility that it is due to a dehydration effect similar to that observed for PAA surfaces, which is discussed below. In any case, variation of wedge test performance with heating time suggested a further test of the model shown in Fig. 13. If the model is correct, we would expect a correlation between incubation times measured for adherends

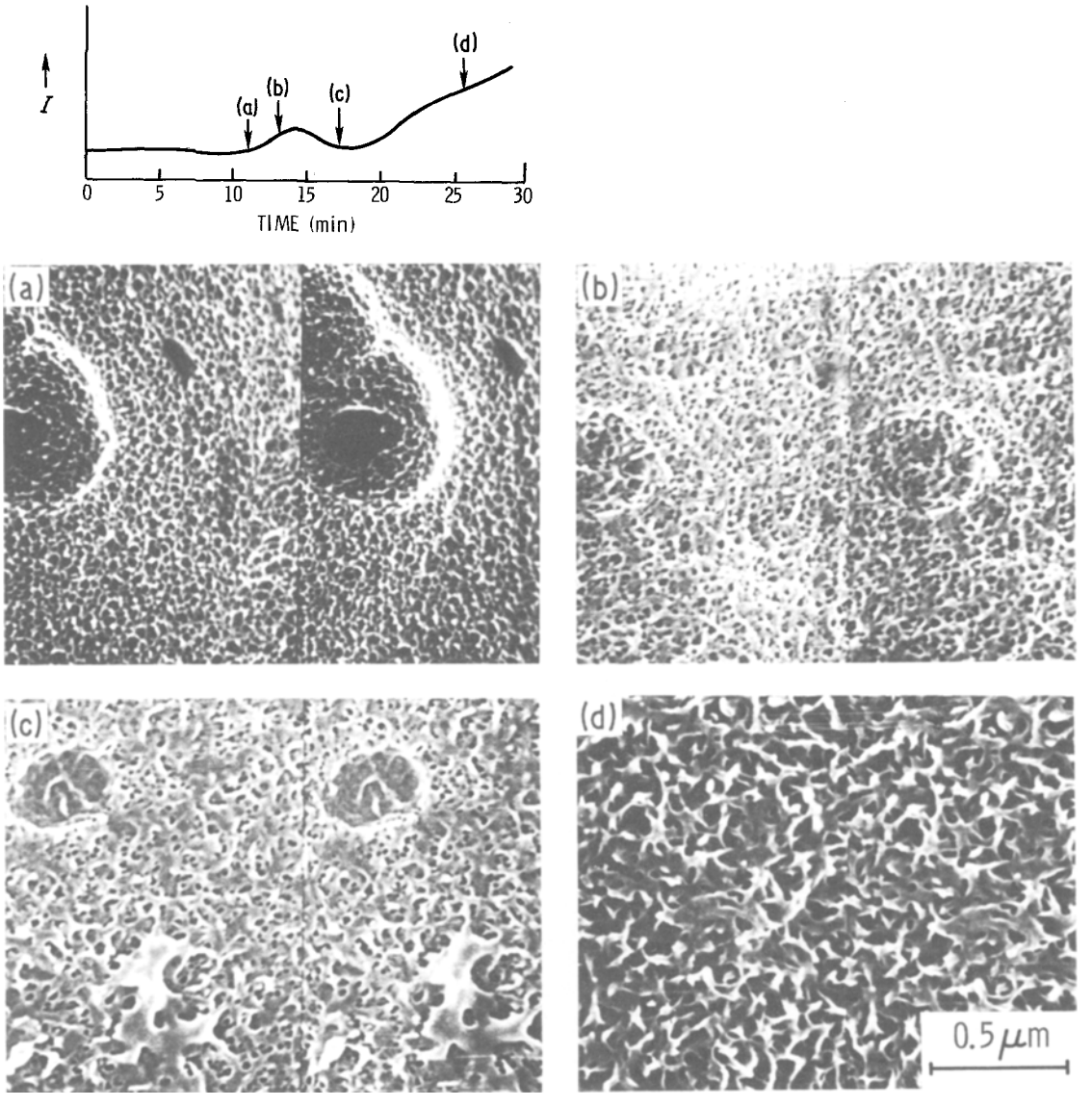

Figure 15 Typical ellipsometer output curve with high-resolution SEM micrographs of FPL sample surfaces removed at various points along the curve: (a) the original FPL morphology; (b) the ellipsometer output has just begun to increase, and the surface morphology shows some filling in of pores; (c) the pseudo-boehmite morphology is beginning; and (d) the surface has completely converted to hydroxide [8].

exposed to different heat treatment times and the wedge test results.

Incubation times measured with the ellipsometer in 80° C water are shown in Fig. 16 adjacent to the wedge test results. There appears to be a correlation between the mechanical property data and surface hydration rates – the longer the incubation time, the better the wedge test performance – which is the first time such a direct correlation has been observed between a bond durability test and a readily measured physical parameter of the adherend.

3.1.2. Surface behaviour diagrams

The large difference observed between the hydration incubation times of FPL and PAA surfaces led us to perform a detailed analysis of these surfaces using XPS. In this work, Davis *et al.* [35] determined that the PAA oxide contained phosphorus in the pentavalent state, presumably in the form of $AlPO_4$, adsorbed on the surface. Since some of our prior work (to be discussed in Section 4) had shown that certain (organic) phosphate compounds were effective hydration inhibitors when adsorbed on Al_2O_3, they then performed

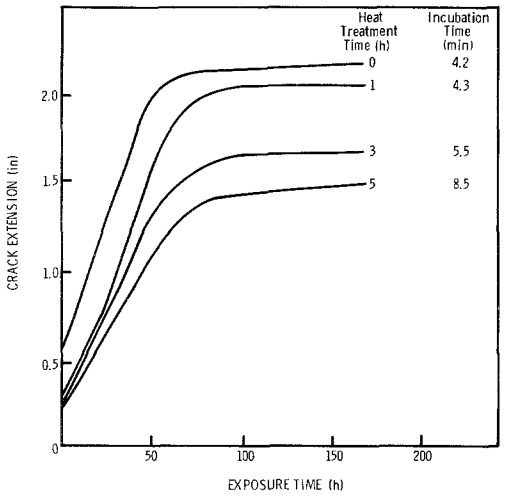

Figure 16 Wedge-crack extension and incubation-time data for 7075 aluminium samples that were heat treated after FPL etching [8].

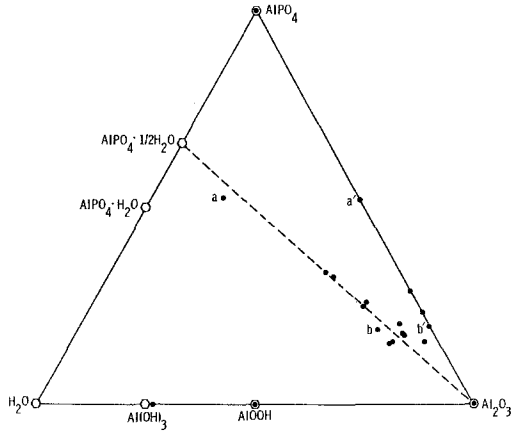

Figure 17 The $AlPO_4$–Al_2O_3–H_2O ternary surface behaviour diagram of the several compounds and fresh PAA oxide surfaces as determined by XPS measurements. The solid points are experimental compositions. The open points are calculated compositions. All surfaces were rinsed in water after anodization. Points a and a′, and b and b′ represent the same coupon before and after dehydration in the UHV chamber (see text) [35].

further investigations to establish the role of the phosphate observed on PAA surfaces.

They measured the aluminium, oxygen, and phosphorus concentrations with XPS using appropriate sensitivity factors and calibration standards to determine surface composition as a function of exposure time to a humid environment, and used these data to calculate the Al_2O_3 and $AlPO_4$ concentrations. By assuming that any excess oxygen was associated with water of hydration, they were able to determine the H_2O content as well. They then plotted these data on Al_2O_3–$AlPO_4$–H_2O ternary surface behaviour diagrams such as those shown in Figs. 17 and 18. This type of diagram, which was originated by Davis *et al.* [35], is analogous to a phase diagram for bulk phases, but is intended to represent effects that are specific to surfaces, e.g. reactions between a surface and its environment or an adsorbate.

The surface behaviour diagram shown in Fig. 17 depicts data obtained from freshly-prepared PAA surfaces. Most of the data cluster at ~ 20% $AlPO_4$ which Davis *et al.* [35] suggest represents approximately one monolayer coverage. Some other data points, e.g. at a, appear to be representative of samples that were not rinsed properly after anodization. The remaining data points lie on the $AlPO_4$–Al_2O_3 tie line and represent samples that contain no water of hydration. These data, however, are not actually characteristic of freshly prepared PAA surfaces but are typical of those htat have undergone extensive dehydration in the vacuum environment of the XPS unit. This effect, which occurs very slowly over a period of days, is demonstrated by the data points pairs a–a′ and b–b′. The unprimed data were taken shortly after insertion of the samples into the XPS vacuum chamber, whereas the primed data were taken three days later.

The real value of plotting data in this unique way on a surface behaviour diagram is that the evolution of surface reactions can be mapped out in exactly the same way as bulk reactions are on

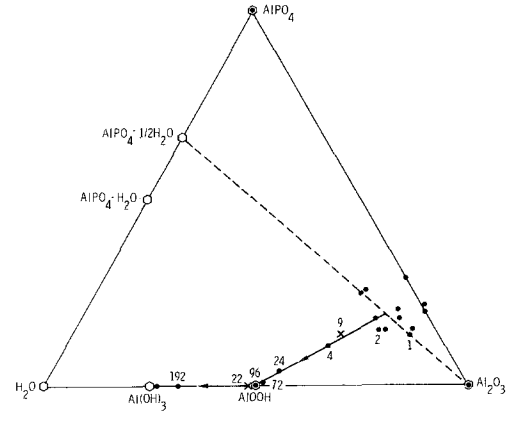

Figure 18 The ternary surface behaviour diagram of fresh and hydrated PAA aluminium oxide surfaces. The cluster of unnumbered points are data taken as freshly prepared surfaces. The numbers by some points denote the exposure time in hours to 100% r.h. at 50° C (solid points) or at 60° C (crosses) [35].

conventional phase diagrams. Thus, Fig. 18 demonstrates what happens to the surface composition of PAA surfaces as a function of exposure time to 100% humidity at 50° C. (The length of exposure time in hours is indicated beside each data point.)

During the first two hours of exposure very little happened to the oxide morphology as observed by XSEM, but the surface composition shifted slightly to the left, indicating a small increase in the H_2O content which probably involves further hydration of the phosphate molecules. For longer exposure times, the composition moved steadily away from the $AlPO_4 \cdot 0.5H_2O$–Al_2O_3 tie line in a straight line until reaching the AlOOH (boehmite) phase at 96 h. From this point on, further exposure caused the composition to change along the Al_2O_3–H_2O tie line toward the most advanced hydration state, i.e. $Al(OH)_3$ (bayerite).

Electron diffraction patterns taken at grazing incidence from these surfaces were completely consistent with the compositions determined by XPS. However, X-ray diffraction patterns and XSEM observations indicated that the surface layer developed during the last stages of hydration exhibited a more complex structure than was implied by the XPS results. In fact, we observed a duplex structure consisting of a sublayer of boehmite and an overlayer of bayerite. Evidently, the bayerite does not grow at the expense of the boehmite but simply nucleates on it and grows as a separate entity under these circumstances.

The evolution of the hydration process exhibited on the behaviour diagram in Fig. 18 has been analyzed by Davis *et al.* [35]. They found a model for the hydration of PAA oxides whose salient features may be summarized as follows:

(a) The first step, which is characterized by a horizontal shift on the behaviour diagram, involves hydration of the surface $AlPO_4$ layer. This process may occur during storage but, since it is reversible, the state of hydration at any given time will depend upon the prior history of the sample. In this regard, we note that the incubation time for hydration of PAA oxides can vary significantly depending upon drying conditions after anodization. For example, Sun [36] noted a factor of two increase in incubation time for samples that were dried with a heat gun compared with those that were tested immediately after anodization and rinsing.

(b) The second step, which moves the surface composition directly toward that of AlOOH, apparently involves slow dissolution of the hydrated phosphate and nearly simultaneous hydration of the oxide with the rate-controlling process that of phosphate dissolution. The conclusion that the phosphate eventually goes into solution, rather than being simply covered over by aluminium hydroxide growth, for example, is consistent with the finding that less than one fifth of the phosphate originally present is detected throughout the boehmite layer of the hydrated surface using Auger depth profiling. Further, the conclusion that phosphate dissolution is the rate-controlling step is supported by the following argument. If rapid phosphate dissolution were followed by slow oxide hydration, the reaction path would evolve along the $AlPO_4 \cdot 0.5H_2O$–Al_2O_3 tie line on the behaviour diagram to Al_2O_3 and then along the Al_2O_3–H_2O tie line to AlOOH. For the situation where the dissolution and hydration rates are more comparable, the path would lie within the triangle at the lower right of the behaviour diagram in Fig. 18. Evidently, the path actually defined by the experimental points is close to the limiting condition of very slow dissolution of the hydrated phosphate followed by rapid hydration of the oxide.

(c) The third step of hydration involves the nucleation and growth of the bayerite phase, which moves the surface composition to the left in Fig. 18 along the Al_2O_3–H_2O tie line, i.e. the normal hydration path of Al_2O_3. As noted previously, X-ray diffraction and XSEM observations suggest that the bayerite nucleates on the platelets of the boehmite phase leading to a duplex layer of bayerite on top of boehmite.

These results, obtained with the aid of surface behaviour diagrams, indicate that the phosphate content of a PAA oxide plays a very significant role in determining the stability of the surface in a moist environment. The conclusion that the dissolution of the phosphate is rate controlling up to the point where the surface layer is transformed to boehmite appears particularly significant. The result, in fact, suggests that the presence of the phosphate is largely, if not totally, responsible for the greater stability of PAA oxides relative to FPL oxides. The concept of monolayer hydration inhibitors that can protect aluminium surfaces from attack by moist environments is thereby introduced. In Section 4 we discuss other work we have done to develop this concept further.

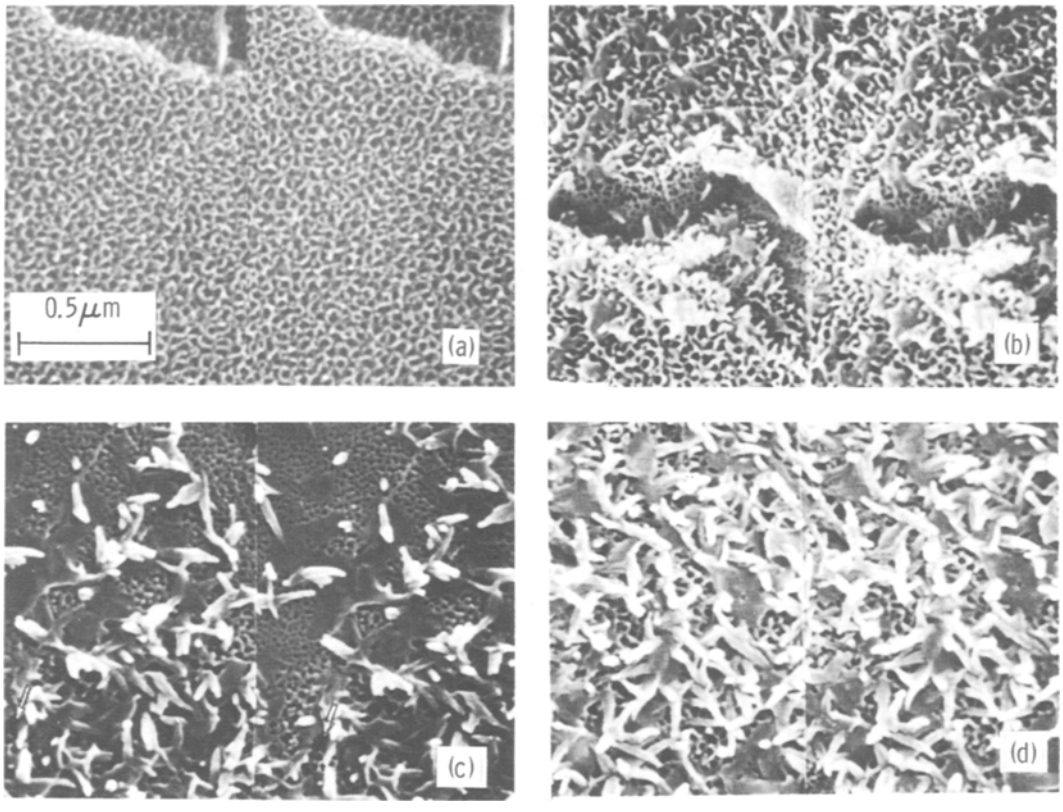

Figure 19 Stereo XSEM micrographs of titanium surfaces prepared by the CAA process and then exposed to water at 80° C for (a) 0, (b) 1, (c) 3, and (d) 4 days. The original oxide, which is amorphous, has converted to anatase, a crystalline form of TiO_2 [38, 39].

3.2. Stability of oxides on titanium

Our studies of oxide stability on titanium, which began with the work of Ditchek *et al.* [24], have shown that all titanium surfaces prepared by the processes discussed in Section 2.2 are much more stable in moist environments than the aluminium surfaces we have investigated. In an attempt to quantify the difference, Natan *et al.* [37–39] investigated the stability of titanium surfaces prepared by the CAA processes and found that when the samples were immersed in water at 80° C, initial morphological change was seen after one-day exposure [38]. (In comparison, an FPL oxide on aluminium would have hydrated in 2 min; a PAA surface in 3 to 5 h).

Using XSEM to examine the exposed surfaces, Ditchek *et al.* [24] and later Natan *et al.* [38, 39] observed a change in morphology from that shown in Fig. 10 to the new structure shown in Fig. 19. The transformed surface shown in Fig. 19 somewhat resembles the hydrated aluminium surface shown in Fig. 12. Upon closer examination, the titanium structure exhibits a needle-like morphology rather than the flake-like morphology of hydrated aluminium surfaces. Moreover, a much more significant difference was found by Natan *et al.* [38], who used electron diffraction to study the nature of the transformation on titanium. In this work, electron diffraction patterns obtained from foils thinned from one side by ion beam milling revealed that the original CAA oxides were primarily amorphous, whereas the needle-like material shown in Fig. 19 was anatase, a tetragonal form of TiO_2. The conclusion that the surface material had undergone a phase transformation with no accompanying chemical change (i.e. oxide to hydroxide) as we observed for aluminium was surprising and raised questions regarding the role of humidity. Later work by Natan *et al.* [39] has demonstrated that although water is not actually incorporated into the transformed product (anatase), its presence during the transformation process profoundly affects the temperature at which it occurs. For example, in the absence of

humidity (r.h. ≈ 0%), the surface oxide remains amorphous and no morphological changes occur at 100° C even after 100 h exposure. On the other hand, when the experiment is done in water at 85° C, marked morphological changes occur, Fig. 19, and the surface oxide converts from amorphous TiO_2 to crystalline anatase after 20 h exposure. Similar observations which suggest that moisture appears to catalyse the amorphous to anatase transformation process (perhaps by a dissolution/reprecipitation process) have been observed previously [40] but not in the context of adhesive bond durability.

The polymorphic transformation that occurs on titanium surfaces might be expected to degrade bond strengths just as the oxide to hydroxide conversion does on aluminium because it also is accompanied by a morphological change. However, because the incubation time for the surface transformation on titanium is so much greater than that for the oxide to hydroxide transformation on aluminium surfaces, we suspected that the transformation on titanium was not a critical factor determining the performance of titanium adherends discussed in Section 2.1.1. Consistent with this expectation, a recent study by Natan *et al.* [38] of failure interfaces on wedge test specimens used to generate the data in Fig. 11, revealed no significant changes in the oxide due to the test, suggesting that surface oxide instability was not a major factor responsible for any of the differences observed in bond durability. Apparently, the Group I and II adherends perform poorly (or marginally) because the interfacial bond strength is determined by chemical forces that are degraded in the presence of humidity, just as we observed for aluminium when mechanical interlocking was not present. On the other hand, the Group III adherends exhibit superior performance because 1. their interlocking oxide morphologies ensure good initial bond strength, and 2. the great stability of their oxides ensures excellent long-term durability. The fact that this combination of properties can be produced on titanium suggests a very bright future for titanium–polymer bond technology. It must be noted, however, that since the use of titanium is indicated only when environmental conditions are too severe for aluminium, that the test conditions should also be increased in severity. Use of more stringent tests for titanium than aluminium would appear appropriate in order to evaluate upper limits on service environments and to identify those areas where improvements might be needed.

4. Hydration inhibitors for aluminium

Our observation that the durability of aluminium–polymer bonds is degraded due to oxide-to-hydroxide conversion even for PAA oxides led us to consider approaches that would impart greater stability to the oxide against the effects of moisture. At the suggestion of Tadros [41], we investigated the use of certain organic compounds that are normally employed as scale inhibitors in recirculating water or steam systems. These inhibitors, which are added directly to the water, apparently function by forming a protective monolayer film on the inside of the metallic parts (pipes, radiators, etc.) that make up the system. Since we desired to protect the oxide in the present case against the effects of moisture without interfering with its interlocking features, the approach of using a monolayer inhibitor seemed attractive. Accordingly, we performed experiments on these compounds to determine (a) whether they could be applied conveniently to FPL and PAA oxide surfaces in monomolecular form, (b) the degree of their effectiveness for inhibiting the oxide-to-hydroxide conversion process when so applied, and (c) whether they remained effective at the oxide–polymer interface after undergoing the heating cycle which is necessary for resin curing.

Among several different types of compounds investigated, we chose nitrilotris (methylene) phosphonic acid (NTMP) [34, 41] for study because we suspected that the deprotonated NTMP molecule (Fig. 20) might bond tenaciously to the aluminium oxide surface replacing adsorbed hydroxyl ions. We wanted to ensure that the NTMP ions were fully ionized in the treatment solution. From titration curves [42] we inferred that the NTMP molecule is multiply ionized at relatively high pH values (pH > 3 to 4), i.e. at values that can be achieved in dilute solutions.

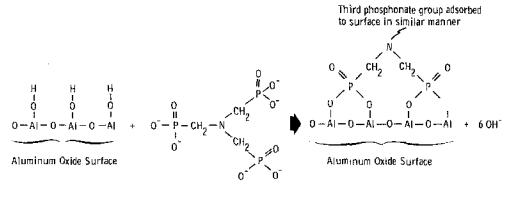

Figure 20 Model for the adsorption of NTMP onto aluminium oxide surfaces. The deprotonated NTMP molecule replaces adsorbed hydroxyl ions, resulting in P–O–Al bonding.

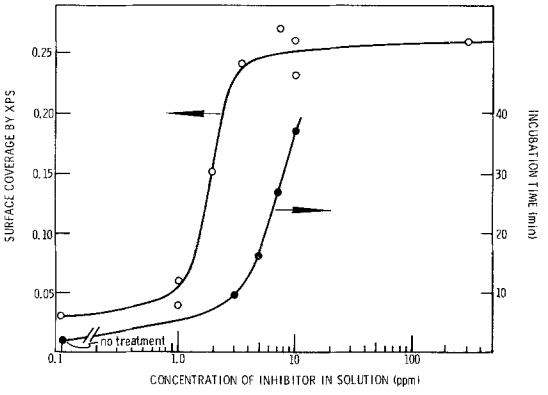

Figure 21 Comparison of surface coverage of NTMP determined from high-resolution ESCA measurements and incubation time determined by ellipsometry.

Accordingly, we studied the surface coverage of phosphonic acid molecules on Al_2O_3 as a function of NTMP concentration in low solute-level aqueous solutions.

After FPL treatment, 2024-T3 aluminium coupons were dipped in aqueous NTMP solutions ranging in concentration from 3 to 300 ppm NTMP, rinsed in deionized water, and dried in flowing air. Surface coverage of the NTMP molecule was determined by measuring the peak height of the 2p photoelectrons from P and Al with XPS and calculating the P/Al ratio using sensitivity factors employed by Davis *et al.* [35]. These data, which are shown in Fig. 21, demonstrate that the NTMP coverage increases markedly when the concentration of the inhibitor in solution reaches the 1 to 10 ppm range. The P/Al ratio saturates at higher solution concentrations suggesting the attainment of monolayer coverage.

We determined the degree of protection against hydration of the treated surfaces afforded by the NTMP coverage using ellipsometry, and hydration incubation times using ellipsometry and XSEM. As can be seen from Fig. 21, the incubation time increases with solution concentration in the same manner as surface coverage except that the two curves are displaced by a factor of four along the NTMP concentration axis. Recent work indicates that at high NTMP solution concentrations all three functional groups of the NTMP molecule are bound to the Al_2O_3 surface whereas at low concentrations only one functional group is involved. This implies that NTMP adsorbed onto the Al_2O_3 surface from very dilute solutions would be less effective in protecting the surface against moisture than NTMP adsorbed from more concentrated solutions. This may explain the displacement of the two curves in Fig. 21. In any event, the data demonstrate that hydration incubation times for FPL oxides can be significantly improved by treatment in aqueous solutions containing greater than 10 ppm NTMP. However, it should be noted that although the incubation time data presented in the figure are rather nicely behaved, considerable experimental scatter has been found at other times during our investigations. We are investigating the possible causes of this scatter and believe some of it relates to the presence of inclusions in 2024 aluminium. In particular, we have observed that hydration of 2024-T3 aluminium (whether treated with NTMP, or untreated) nucleates at CuAl inclusions (Fig. 22). This sample was removed from its 80° C water environment just as the ellipsometry trace

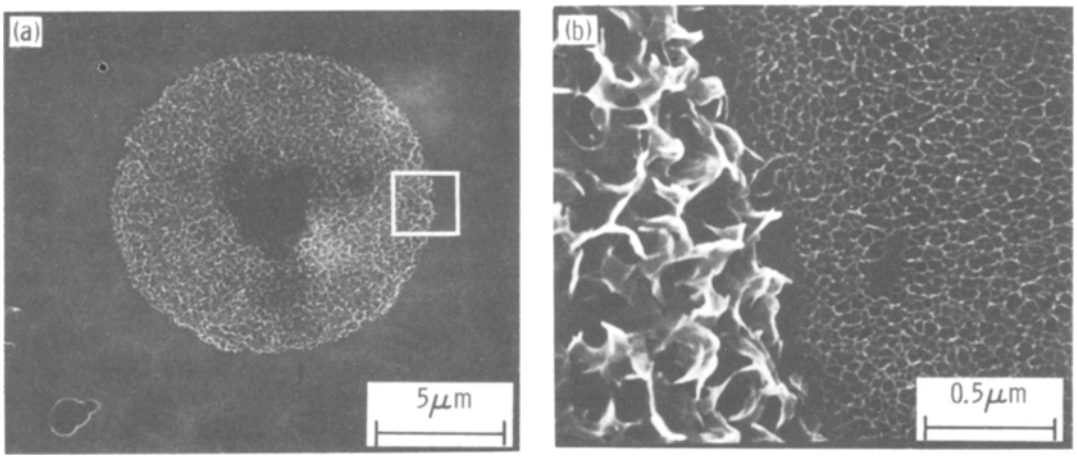

Figure 22 XSEM micrographs of a hydration "island" surrounding an AlCu inclusion at (a) medium and (b) high magnification. The original FPL oxide is visible to the right in (b).

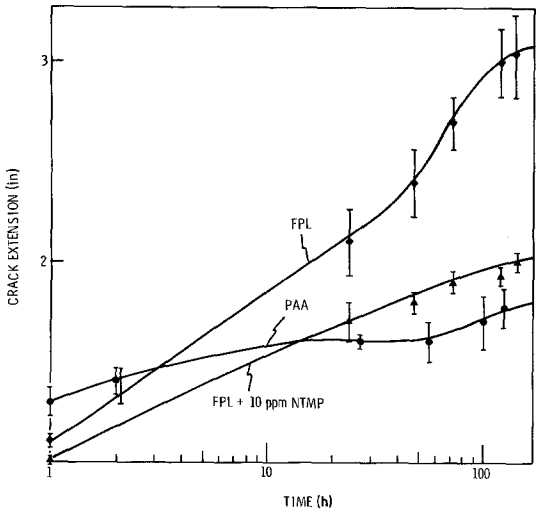

Figure 23 Wedge-test crack length as a function of exposure time in a humidity chamber at 100% r.h., 60° C. The data demonstrate that the performance of FPL-treated adherends under these test conditions is improved significantly when the adherend is treated before bonding in an inhibitor solution containing just 10 ppm. In fact, after the treatment, the performance approaches that of PAA-treated adherends [34].

showed signs of early hydration activity. When it was examined by XSEM we observed circular patches of hydration product, as shown in the figure. Chemical analysis by energy dispersive spectroscopy (EDS) revealed a very high Cu content at the centre of each hydration patch, approaching that consistent with a CuAl inclusion. The inclusion sites might be particularly difficult to passivate because of local galvanic currents and/or discontinuous aluminium oxide film. Even though inclusions might lead to scatter in the incubation time data, the NTMP inhibitor always improves the incubation time (for solution concentrations greater than 10 ppm) by a significant factor. Work is currently in progress to define more precisely approaches for eliminating the observed variability.

To test whether the inhibitor retains its effectiveness for treated aluminium surfaces bonded to thermoset polymers, we performed wedge tests on adherends processed in the following manner: Test panels ($6 \times 8 \times \frac{1}{8}$ in) were treated by the FPL or PAA process, dipped for 15 min in aqueous solutions containing 200 to 300 ppm of NTMP, rinsed vigorously in distilled water, dried, and bonded together using a water-wicking adhesive (American Cyanamid FM 123-2) and a pressure of 40 psi held for 1 h at 120° C and cooled under

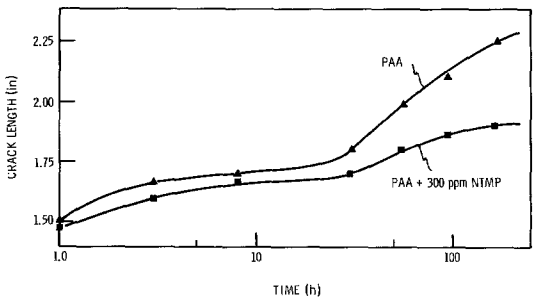

Figure 24 Wedge-test crack length as a function of exposure time in a humidity chamber at 100% r.h., 60° C showing the improvement in performance when PAA adherends are treated with NTMP inhibitor [43].

pressure. After this, the bonded panels were cut into 1 x 6 in test pieces and the samples subjected to a standardized wedge test [31], the results of which are shown in Fig. 23.

It is evident that this simple inhibitor treatment improves the bond durability of adhesively bonded aluminium structures. In fact, the data demonstrate that the wedge test performance of FPL adherends treated with the NTMP inhibitor is so improved that it is comparable to that of PAA adherends. Moreover, recent work indicates that significant improvements can be obtained for PAA adherends using the NTMP inhibitor treatment also [43]. In this study, we have observed that the P/Al ratio determined by XPS on PAA oxides increases from P/Al = 0.14 for untreated surfaces, to P/Al = 0.25 for surfaces treated in aqueous solutions containing greater than ~ 100 ppm NTMP. The phosphorous concentration on treated PAA surfaces corresponds closely to that observed on FPL oxides treated in the same manner but we are not yet sure of the phosphate/phosphonic acid molecule ratios. Nonetheless, the NTMP treatment does improve wedge test performance of PAA adherends under these test conditions as it does for FPL adherends (Fig. 24).

These preliminary data provide additional support for the proposed model, Fig. 13, which suggests that the oxide to hydroxide conversion process is responsible for the degradation of aluminium–polymer bonds in humid environments. Thus, in this aspect of the work, we have again demonstrated a definite correlation between incubation times and bond durability. In addition, the results suggest that the use of organic inhibitors to retard hydration rates on aluminium is an approach that shows considerable promise for

improving the long-term durability of adhesively bonded aluminium structures. However, it must be noted that considerably more research is needed before this approach can be used for service applications. Specifically, more tests are needed to evaluate the degree of compatibility between organic inhibitors and the large number of adhesives that are currently employed in the aerospace industry. The present work suggests that the presence of a monolayer NTMP inhibitor is compatible with the epoxy adhesive used, but further tests are needed to determine whether the results can be extrapolated to other epoxies. We also note that NTMP is not compatible with phenolic-type primers such as EC-1660; in this case the presence of NTMP appears to weaken the bond strength as determined by a T-peel test [44]. Even so, the present work demonstrates that organic inhibitors, when used in monolayer form on the adherend as in this study, or perhaps by incorporation within the primer, may provide attractive alternatives to inorganic inhibitors (e.g. chromates) which have been used in the past to improve the performance of adhesively bonded aluminium structures in humid environments.

5. Discussion and conclusions

This paper is a review of the results of a comprehensive investigation made at the author's laboratories to determine those factors responsible for promoting the integrity and long-term durability of metal–polymer bonds used in the fabrication of aircraft and aerospace structures. Using a multidisciplinary approach and a variety of surface analytical techniques, e.g. XSEM, XPS, ellipsometry, and surface behaviour diagrams, we have evolved several important concepts:

(a) The initial integrity of metal–polymer bonds used for structural applications depends critically upon the morphology of the surface oxide on the metal. In the case of aluminium and titanium, we have observed that certain etching or anodization pretreatment processes produce oxide films on the metal surfaces which, because of their porosity and microscopic roughness, mechanically interlock with the polymer forming much stronger bonds than if the surface were smooth. Indeed, evidence is presented that this type of bond fails (in the absence of environmental effects) only when the polymer itself fails by viscoelastic deformation. In contrast, we observe that when the oxide lacks these morphological features, and bond strength is determined solely by chemical forces across the interface, separation can occur rather cleanly at the interface at stress levels which may be entirely inadequate for structural applications.

(b) The long-term durability of metal–polymer bonds is determined to a great extent by the environmental stability (or lack of stability) of the same oxide that is responsible for promoting good initial bond strength. For aluminium, moisture intrusion at the bond line causes the oxide to convert to a hydroxide with an accompanying drastic change in morphology. The resulting hydrated material adheres poorly to the aluminium beneath it and, therefore, once it forms, the overall bond strength may be severely degraded. Oxides formed on titanium are much more stable than those on aluminium but under some circumstances the originally amorphous oxide undergoes a polymorphic transformation to anatase. Because of volume changes and accompanying morphological changes this transformation might lead to bond degradation just as the oxide to hydroxide conversion process does for bonds to aluminium. The transformation is highly temperature and moisture dependent and is being studied further because it could become an important degradation mechanism in future applications where attempts are made to increase service temperatures through the use of polyimide adhesives, for example.

(c) The proposed degradation model for aluminium–polymer bonds is supported by evidence that shows a correlation between incubation times for the oxide-to-hydroxide conversion process and wedge test results; the longer the incubation time of oxides prepared (and treated) in various ways, the better the wedge test results. This appears to be the first time that such a direct correlation has been observed between a bond durability test and a measurable physical parameter of the metal adherend.

(d) A new technique, the surface behaviour diagram, was developed during this work. This type of diagram is analogous to phase diagrams for bulk phases but is intended to represent effects that are specific for surfaces, e.g. reactions between a surface, an adsorbate, and the environment. In the present case, the technique was used to show that the greater stability of PAA surface oxides, relative to FPL oxides, is due to the presence of adsorbed phosphate (from the electrolyte) which

inhibits the oxide/hydroxide conversion process until the phosphate itself becomes extensively hydrated and is lost by dissolution. This example suggests that the technique may be generally useful for surface science studies particularly in the field of metal corrosion and corrosion inhibition.

(e) Durability of adhesive bonds to aluminium can be significantly improved by an extremely simple treatment in which monolayer films of certain organic acids are applied to the adherend oxide to protect it against moisture effects. Specifically, we have shown that an adsorbed monolayer of an amino phosphonic acid can improve the stability of FPL-treated aluminium so that its performance in wedge tests is comparable to that of aluminium treated by the PAA process. Moreover, oxides formed on aluminium by the PAA process, which are normally stabilized to some extent against moisture by adsorbed phosphate, can be more effectively stabilized by the amino phosphonic acid treatment. The attractiveness of the inhibitor treatment is enhanced by the fact that since the inhibitor is used in monolayer form, only small quantities are needed to treat very large quantities of aluminium.

Another potential approach for improving durability is suggested by the observation that crystalline Al_2O_3, whether in the form of powders or single crystals, is very much more stable than the FPL or PAA oxides which we have determined are amorphous by electron diffraction. Hydration of amorphous oxides was observed in a matter of minutes or hours when immersed in 80° C water, but none was found by XSEM on crystalline material that had been exposed for over a week in water heated to temperatures up to the boiling point. Evidently, the degree of crystallinity of Al_2O_3 profoundly influences its stability against the effects of moisture. Clearly, this suggests another avenue of investigation for improving the performance of metal–polymer bonded structures.

(f) Although the emphasis of this work has been on metal–polymer bonds, its implications extend beyond this technology area. Specifically, the work on durability has clear relevance to the general field of corrosion and corrosion inhibition as follows: The reaction between water and a surface oxide to form a hydroxide cannot be considered strictly a corrosion process because the metal itself is not attacked in the initial stages. Nevertheless, we suggest that it is an important precursor step leading to eventual corrosion. In support of this belief, we have already noted in Section 3.1.2 that when an aluminium sample is exposed to water, the oxide film initially passivates and protects the metal from attack during an "incubation" period. Intense hydration activity then occurs which converts the original oxide to a hydroxide. Only after hydroxylation do we observe evidence of true corrosion, i.e. when gas evolution begins, suggesting that the aluminium metal itself is reacting with the water to form a hydroxide and hydrogen gas. Evidently, the protection provided by the oxide layer is disrupted once the oxide hydrates, suggesting that procedures designed to reduce the rate of hydroxylation would be effective in corrosion protection of aluminium also. If so, we suggest that the concepts and techniques developed during these investigations could be of considerable benefit if properly applied to the general field of metal protection against environmentally induced degradation.

Acknowledgements

The author wishes to thank Dr Surya P. Kodali for his support and Dr Dallis A. Hardwick, now at the Los Alamos National Laboratories, and Mr David K. McNamara for assistance in preparing the manuscript. Thanks are also due to the following agencies for supporting the indicated aspects of this work: The surface behaviour diagram work was performed under contract F49520-78-C-0097 to AFOSR; the titanium work under contract N00019-80-C-0508 to NASC; the inhibitor work under contract N00014-80-C-0718 to ONR/AROD.

References

1. H. W. EICHNER and W. E. SCHOWALTER, Forest Products Laboratory, Madison, WI, Report No. 1813 (1950).
2. G. S. KABAYASHI and D. J. DONNELLY, Boeing Co., Seattle, WA, Report No. DG-41517 (February, 1974).
3. Fokker-VFW, Amsterdam, The Netherlands, Process Specification TH 6.785 (August, 1978).
4. R. F. WEGMAN and M. J. BONDNAR, *SAMPE Q.* 5 (1973) 28.
5. M. J. FELSEN, Proceedings of the 10th National SAMPE Technical Conference, Kiamesha Lake, NY, October 1978 (SAMPE, Azusa, CA, 1978) p. 100.
6. P. F. A. BIJLMER, *J. Adhes.* 5 (1973) 319.
7. J. D. VENABLES, D. K. McNAMARA, J. M. CHEN, T. S. SUN and R. L. HOPPING, *Appl. Surf. Sci.* 3 (1979) 88.
8. J. D. VENABLES, D. K. McNAMARA, J. M. CHEN,

B. M. DITCHEK, T. I. MORGENTHALER, T. S. SUN and R. L. HOPPING, Proceedings of the 12th National SAMPE Technical Conference, Seattle, WA, October 1980 (SAMPE, Azusa, CA, 1980) p. 909.
9. A. J. KINLOCH, *J. Mater. Sci.* **15** (1980) 2141.
10. *Idem, ibid.* **17** (1982) 617.
11. D. K. McNAMARA, Martin Marietta Laboratories, Baltimore, MD, unpublished work (May 1979).
12. ASTM Standard D1781, Annual Book of ASTM Standards, Part 22 (ASTM, Philadelphia, PA, 1980) p. 587.
13. B. V. DERYAGIN and M. S. METSIK, *Sov. Phys. Solid State* **1** (1960) 1393.
14. J. M. CHEN, T. S. SUN, J. D. VENABLES and R. L. HOPPING, Proceedings of the 22nd National SAMPE Symposium, San Diego, CA, April 1977 (SAMPE, Azusa, CA, 1977) p. 25.
15. J. J. BICKERMAN, "The Science of Adhesive Joints" (Academic Press, NY) 1968.
16. D. H. KAEBLE, *SAMPE Q.* 7 (1976) 30.
17. W. BROCKMAN, Proceedings of the 21st National SAMPE Symposium, Los Angeles, CA, April 1976 (SAMPE, Azusa, CA, 1976) p. 30.
18. W. BROCKMAN and H. KOLLECK, Proceedings of the 23rd National SAMPE Symposium, Anaheim, CA, May 1978 (SAMPE, Azusa, CA, 1978) p. 119.
19. E. H. ANDREWS and N. E. KING, *J. Mater. Sci.* **11** (1976) 2004.
20. T. P. HOAR and N. F. MOTT, *J. Phys. Chem. Solid* 9 (1959) 97.
21. D. K. McNAMARA, Martin Marietta Laboratories, Baltimore, MD, unpublished work (September 1979).
22. J. S. AHEARN, T. S. SUN, C. FROEDE, J. D. VENABLES and R. L. HOPPING, *SAMPE Q.* **12** (1980) 39.
23. D. A. VERMILYEA and W. VEDDER, *Trans. Faraday Soc.* **66** (1970) 2644.
24. B. M. DITCHEK, K. R. BREEN, T. S. SUN and J. D. VENABLES, Proceedings of the 12th SAMPE Technical Conference, Seattle, WA, October 1980, edited by M. Smith (SAMPE, Azusa, CA, 1980) p. 882.
25. S. R. BROWN, in Proceedings of the 27th National SAMPE Symposium, San Diego, CA, May 1982 (SAMPE, Azusa, CA, 1982) p. 363.
26. S. R. BROWN and G. J. PILLA, Naval Air Development Command, Warminster, PA, Report NADC-82032-60, March 1982.
27. G. W. LIVELY, Air Force Materials Lab., Dayton, OH, Report AFML-TR-73-270, Part I, January 1974.
28. Y. MOJI and J. A. MARCEAU, US Patent 3,959,091, May 1976.
29. A. W. BETHUNE, *SAMPE J.* **11** (3) (1975) 4.
30. J. A. MARCEAU, Y. MOJI and J. C. McMILLAN, Proceedings of the 21st National SAMPE Symposium, Los Angeles, CA, April 1976 (SAMPE, Azusa, CA, 1976) p. 332.
31. ASTM Standard D3762, Annual Book of ASTM Standards, part 22 (ASTM, Philadelphia, PA, 1980) p. 1037.
32. A. MAHOON and J. COTTER, Proceedings of the 10th National SAMPE Technical Conference, Kiamesha Lake, NY, October 1978 (SAMPE, Azusa, CA, 1978) p. 425.
33. W. VEDDER and D. A. VERMILYEA, *Trans. Faraday Soc.* **65** (1969) 561.
34. J. S. AHEARN, G. D. DAVIS, T. S. SUN and J. D. VENABLES, Proceedings of the Symposium on Adhesion Aspects of Polymer Coatings, Minneapolis, MN, May 1981, edited by K. Mittal (Plenum Pub. Co., New York, NY, 1983) p. 288.
35. G. D. DAVIS, T. S. SUN, J. S. AHEARN and J. D. VENABLES, *J. Mater. Sci.* **17** (1982) 1807.
36. T. S. SUN, Technical Report TR80-34c, Martin Marietta Laboratories, Baltimore, MD, September 1980.
37. M. NATAN, J. D. VENABLES and K. R. BREEN, Proceedings of the 27th National SAMPE Symposium, San Diego, CA, May 1982 (SAMPE, Azusa, CA, 1982) p. 178.
38. M. NATAN and J. D. VENABLES, *Electrochem. Soc. Extended Abstr.* **83** (1983) 379.
39. *Idem, J. Adhes.* **15** (1983) 125.
40. A. C. FRAKER and A. W. RUFF, *Corros. Sci.* **11** (1971) 763.
41. J. D. VENABLES, M. E. TADROS and B. M. DITCHEK, US Patent 4,308,079.
42 R. P. CARTER, R. L. CARROLL and R. R. IRANI, *Inorg. Chem.* 6 (5) (1967) 939.
43. D. A. HARDWICK, J. S. AHEARN and J. D. VENABLES, Second-year report to Office of Naval Research, Boston, MA, ONR Contract N00014-00-C-0718, November 1982.
44. ASTM Standard D1876, Annual Book of ASTM Standards (ASTM, Philadelphia, PA, 1980) p. 607.

Received 26 October
and accepted 20 December 1983